GEOSCIENCES

Thermostructural Evaluation of the Muriaé Watershed (Rio de Janeiro portion)

SUZE N.P. GUIMARÃES, FÁBIO P. VIEIRA & HELLEN R. BARBOZA

Abstract: The hydrological basins can be considered sources of relevant information about the evolution of the Earth's crust since the relief forms that define the hydrographic channels are the resultant of the interaction between tectonics, pedogenics, intemperics and thermals processes. The geothermal field of Muriaé watershed was evaluated using eight (8) thermal logs and twenty-two (22) geochemical logs. The structural lineaments evidenced on the surface were interpreted jointly with the identification of sixty-five (65) magnetic lineaments from airborne magnetic data interpretation. The depths of these structures were range from the surface up to 4.5 km. The interpreted data allowed identification of regional tectonics features in the NE-SW direction, where the identified magnetic lineaments show a spatial correlation with accentuated topographic structures. The differences in the depths of the magnetic bodies found in conjunction with the heat flow distribution, evidence two distinct thermostructural zones: A1 (east part) presenting heat flow values within the average (approximately $60\frac{mW}{m^2}$) and magnetics sources varying between 3-8 km in-depth. While the A2 (western), has anomalous heat flow ($80\frac{mW}{m^2}$ on average) and shallower magnetic sources, varying between 4-5 km.

Key words: Curie surface, geothermal, magnetic lineaments, Muriaé watershed, thermostructure.

INTRODUCTION

Geophysics coupled with geological knowledge seeks to mitigate ambiguities and minimize errors in the interpretation of a region of interest. This gives a good understanding of different parts of the Earth's crust. For regional scale studies, geophysical methods are important for highlighting structures such as faults, folds, crystalline basement and the limits of sedimentary basins, actively contributing to the geological/geophysical interpretation (Kellogg 1953, Blakely 1996, Kearey et al. 2009).

One of the geophysical methods used in the characterization of crust is the geothermal method, which consists of the set of techniques that study and explore the terrestrial heat. At the Earth's surface, the main contribution to geothermal energy comes from the heat of solar radiation (Cerrone & Hamza 2003) while, in the deeper layers, it comes from various subsurface sources such as volcanic zones, the edges of tectonic plates and/or places that have some crust thermotectonic heterogeneity (Benfenatti 2017). The study of the thermal regime of the Earth's interior is of great importance for its structural knowledge since tectonism and geological formations are connected to the thermal history of the rocks. In addition, thermal history of the rock formation can also be assembled from thermal

logs, as in Hamza & Verma (1969), who correlated the ages of the basement rocks of the USA, Canadá, Austrália and Índia with the heat flow behavior of their sites.

A complementary geophysical method to geothermal studies is the magnetometry. It can be said that this method is based on the magnetic susceptibility study of the crustal rocks. Evaluating the different types of materials and variations of such physics properties in different types of rocks (Kearey et al. 2009).

Over the years, studies with geological, hydrological and environmental character on the Muriaé watershed have been carried out as in Prado et al. (2005). They studied the physical environment of this basin, aggregating information such as weather, geology, water resources, pedology, geomorphology and land use with the objective of support family-based farmers in the transition to sustainable agriculture.

Amorim et al. (2017) mapped the geosystems and anthropic systems in their study of areas for the risk of flooding in the lower Muriaé watershed. With this, it became possible to identify natural and social elements that highlighted the risk of inundation and flooding, as well as their period/frequency and intensities. Salviano (2019) performed a hydrological modeling of the basin in order to promote predictions of river levels to avoid damage from possible flooding.

In this research, the main objective was to map structural and tectonic features to evaluate the watershed lithosphere. Characterizing distinct thermomagnetic zones, through a geothermal and magnetic analysis of the upper crust. It began with the evaluation of thirty well with thermal logs information, measured directly and indirectly (by geochemical measurements). These temperatures data are linked to their respective thermal conductivity values and enabled the mapping of the heat flow of the region. Was made an evaluation of the available airborne magnetic data made available by CPRM (Brazilian Geological Service), so that, from anomalous magnetic field data, could be identified and classified the subsurface magnetic sources of tectono-structural interest.

GEOLOGICAL AND GEOMORPHOLOGICAL CONTEXT OF THE MURIAÉ WATERSHED

The rupture of Gondwana and the opening of South Atlantic, between the Upper Jurassic (157.3-145 Ma) and Lower Cretaceous (145-100.5 Ma), stands out as the most important tectonic event that defined the Brazilian Cenozoic landscape (relief). This event is well marked along the coastal portion of the south and southeastern regions of Brazil. In this place, its action was more intense and generated a large initial crustal arching in a row the rifting processes that generated the Mar and Mantiqueira mountain. These tectonics events de fines the Brazilian Atlantic plateau (Riccomini 1989).

This context was established predominantly along the great traces of the NE-directed Precambrian alkaline lineaments (Sadowski & Campanha 2004), branching for more than 2,000 km in extension between the states of the southern to southeastern region of Brazil, reactivated as faults during Cretaceous and Cenozoic. Thus, the compartmentalization of the relief, as well as the fluvial dynamics, are preferentially controlled by such structures.

The Rio de Janeiro state is localized in southest region of Brazil, and its geological context envoling the Mantiqueira structural province, which age ranges from late Neoproterozoic to early Paleozoic (680-480 Ma), with a predominantly *NNE* to *SSW* orientation along the Atlantic coast (Almeida 1976). The Muriaé watershed under study is in the NE region of Rio de Janeiro, comprising part

of the Atlantic orogenic belt. This morpho-structural units comprises a diverse set of metamorphic and igneous rocks of Precambrian and Paleozoic age. Such rocks, included in the Ribeira folding zone, were subjected to different orogenic cycles, ending with the Brasiliano event, at the end of the Proterozoic (Heilbron 1995).

The tectonic context of this region is mainly marked by a series of normal faults and coastal massifs that have supported some zones of plateau and interplanaltic depressions. Frequently, the depression area presents a series of mountainous alignments that behave as steps of by lithological and structural conditions (Coelho Netto 1997), this is observed in a section of the South Paraiba river valley.
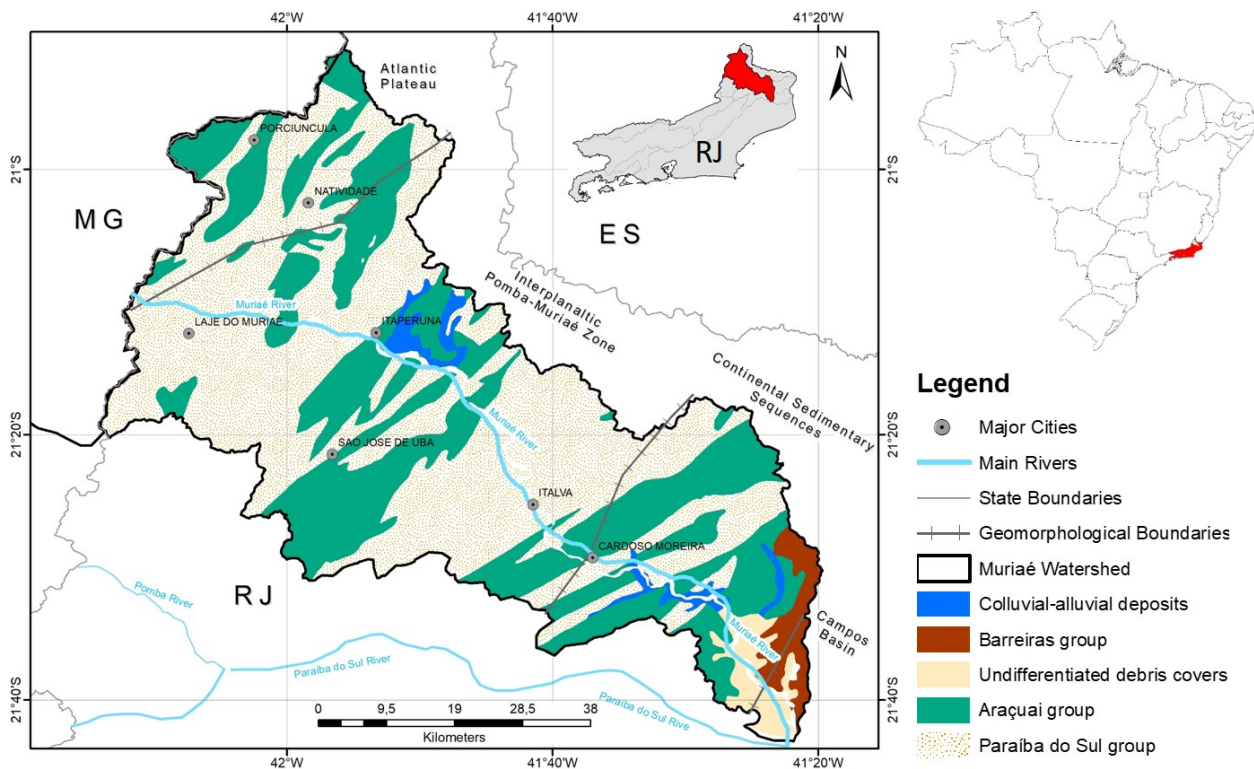
Figure 1. Simplified geology and main morpho-structural domains of the Rio de Janeiro part of the Muriaé watershed. Modified from Bizzi et al. (2003).

The geological units that mark the study region are predominantly the Araçuaí and Paraíba do Sul groups (Figure 1). In the southeast region of the basin, there is the presence of Quaternary units formed by undifferentiated detrital covers and the Barreiras unit. These set of rocks with different resistance to erosive processes and denudation gave rise to the relief forms in the study area: mountain cliff, mounds and hills (Dantas 2001). Its geomorphological context is an interplanaltic Pomba-Muriaé zone, where the local tectonism presents faults and fractures in a NE-SW direction in the central-south portion of the basin and in an NNE-SSE direction in the central-north portion. The rocks of this basin are predominantly orthoderivative (igneous) in the northern part and paraderivative (sedimentary) in the southern part of the basin (Brenner et al. 1980).

MATERIALS AND METHODS

The methodologies used in this research are based on the solutions of fundamental equations that control the thermal and magnetic behavior in the study region. The temperature distribution in crust is a tracer in heat flow measurements with mantelic origin since temperature is a robust parameter for tracking of the geothermal gradient. The use of magnetic information of rocks, on the other hand, allows the contrasts of different magnetic properties coming from the interior in the Earth.

Geothermal Method

Temperature and Geothermal Gradient

It is possible to determine the geothermal gradient of a region using direct and indirect methods. The direct method consists of temperature measurements by thermal logging, i.e., in-depth temperature loggers that allow response times in the order of seconds. The indirect estimates are used to obtain information about temperatures depth when it is not possible perform thermal logging. For example, the knowledge of the dissolved element content in groundwater that allows the determination of the geothermal reservoir temperature in the subsurface (Bullard 1939, Boldizsar 1958, Swanberg & Morgan 1980, Haenel et al. 1988).

In this research, we used the direct method of temperature measurements at depth designated: *Conventional Bottom-Hole Temperature* (CBT), being used for cases in which the fluid flow inside the well disturbs the conductive thermal regime (Hamza & Muñoz 1996). In this case, the relationship between the downhole temperature (T_{CBT}) and the annual average temperature at the surface (T_0), which results in the geothermal gradient of that environment, is determined by the following equation:

$$\Gamma = \frac{T_{CBT} - T_0}{Z_{CBT} - Z_0} \tag{1}$$

where, the term on the right side represents the thermal gradient (Γ), Z_{CBT} is the depth of the well base under analysis and Z_0 is a surface depth.

Thermal Conductivity

The thermal conductivity data refer of measurements performed on core samples from the main lithology types of the region in the Rio de Janeiro state. The values were compiled by Hamza & Gomes (2003) and presented in Table I. The mean thermal conductivity values to each well were calculated using information about its lithological profile. These basing in the weighted average between the product of lithotype thicknesses and values representing the thermal conductivity.

Estimates of Heat Flow

Expressed by *Fourier's* law for thermal diffusion (Özisik 1993), the heat flow values were calculated as the product of the geothermal gradient (Γ) by the representative average thermal conductivity (λ) calculated for each well, as illustrated in the equation below:

$$q = -\lambda \frac{\partial T}{\partial z} \tag{2}$$

Table I. Thermal conductivity values (in $\frac{W}{m.K}$) of the main lithotypes found in regions of the Rio de Janeiro state according to Gomes & Hamza (2003).

Lithological type	Thermal conductivity	Lithological Type	Thermal conductivity
sand	2.8	granitic gneiss	3.1
clayey sand	2.2	leucocratic gneiss	2.8
sandstone	2.7	mesograph gneiss	3.9
sedimentar unclassified	2.7	gneiss grenade	4.4
river sedimentar	2.7	granulate	3.3
siltstone	2.7	granite	3.1
amphibolite	3.3	differentiated granite	2.7
calc-silicate	2.4	porphyritic granite	2.6
quartzite	3.1	granitoid	3.0
biotite gneiss	3.5	totalitic granitoid	3.1
banded gneiss	3.0	diabase	2.6
phacoidal gneiss	4.3	crustalline not identified	2.9

where q is the heat flow density per unit area ($\frac{mW}{m^2}$), ∂T is the temperature variation along the log (^{0}C), ∂z is the difference between the well bottom depth and the surface (m) and λ is the average thermal conductivity ($\frac{W}{mK}$). The direction of heat flow is always from the warmer to the colder medium, positive vertically upwards. As the heat flow is opposite to the geothermal gradient (which is positive towards the terrestrial interior).

Magnetometric Method

The main purpose of this method is to provide magnetic information on both surface and subsurface rock, with a wide range of applications, from small-scale surveys, such as in engineering and archeology, to regional geological studies for the purpose of prospecting for mineral resources. For a more comprehensive study, aircraft surveys are used. Thus, the airborne magnetometry methods are often used for detailed and semi-detail regional studies. From the information of the Anomaly Magnetic Field (AMF), measured in airborne surveys, filtered and already processed, geophysical techniques are used to interpret the results and cross-reference them with the local geology.

Vertical Derivative

Vertical Derivative Convolution (Gunn 1975) is a geophysical technique based on the application of directional filters in the AMF. The derivative spatial filtering is used to sharpen the edges of anomalies and enhance shallow features, this filter is the vector resulting from the enhancement of the high frequencies of the magnetic signal, where the magnetic anomaly ($\overrightarrow{AMF}$) is linearly transformed by means of the first derivative of the vertical component (*z*).

It can be shown that the vertical derivative of order n is equal to the Fourier transform of the AMF multiplied by the wavenumber (k) raised to n, i.e., (k^n) and the wavenumber is a parameter basing in the your spatial combination (x and y directions). By Fourier theory, it is known that the vertical derivative of a potential field, such as AMF can be computed using the following relation:

$$\Im \left(\frac{\delta^n AMF}{\delta z^n} \right) = |k|^n \, \Im \, [AMF] \tag{3}$$

$$k = \sqrt{\left(k_x \right)^2 + \left(k_y \right)^2} \tag{4}$$

The vertical derivative map is more responsive to local influences than broad or regional effects. This result tends to give sharper picture in comparison the map of the total field intensity. The smaller anomalies are more readily apparent in area of strong regional disturbances. In fact, the first vertical derivative is used to delineate high frequency features more clearly where they are shadowed by large amplitude, low frequency anomalies. In the present investigation, vertical derivative techniques were applied by using Oasis Montaj package by Geosoft software.

Analytic Signal Amplitude

The analytic signal technique (Nabighian 1972, Roest et al. 1992, Blakely 1996) where it is possible to calculate the amplitude or phase of a signal. This amplitude technique uses the square root of the sum of the squares of the directional derivatives of the analytic field studied. Nabighian (1972) has shown that for two-dimensional bodies, a bell-shaped symmetrical function can be derived which maximizes exactly over the top of the magnetic contact. The three-dimensional case was derived in 1984 also by Nabighian. This function is the amplitude of the analytical signal. The only assumptions made are uniform magnetization and that the cross-section of all causative bodies can be represented by polygons of finite or infinite depth extent. This function and it derivative are, therefore, independent of strike, dip, magnetic declination, inclination and remanent magnetism (Li 2006).

The 3D analytical signal, A, of a potential field anomaly can be defined (Nabighian 1984).

$$A \left(x, y, z \right) = \sqrt{\left| \frac{\partial B}{\partial x} \right|^2 + \left| \frac{\partial B}{\partial y} \right|^2 + \left| \frac{\partial B}{\partial z} \right|^2} \tag{5}$$

In this case, A refers to the amplitude of the analytical signal and $\overrightarrow{AMF}$ to the anomalous magnetic field where the technique was applied. This amplitude *(A)* has a bell-shape about anomaly-causing sources that depend only on their spatial locations and not their magnetization directions, so this tool is used to delimit anomaly edges.

Euler Deconvolution

Euler deconvolution is the geophysical technique used to extract depth and horizontal location of magnetic sources. Its result is independent of the direction and inclination of the geomagnetic field, and the orientation of the source magnetization, thus it is relatively insensitive to small field distortions (Thompson 1982, Reid et al. 1990, Clark 1997). In general, Euler deconvolution is based on applying the homogeneous Euler equation through a moving window for a given structural index (η).

Considering $\vec{T}$ as the total magnetic field measured at the position (x, y, z), we can write the *Euler* equation as follows:

$$(x - x_o)\frac{\partial \vec{T}}{\partial x} + (y - y_o)\frac{\partial \vec{T}}{\partial y} + (z - z_o)\frac{\partial \vec{T}}{\partial z} = \eta\left(\vec{B} - \vec{T}\right) \tag{6}$$

where in (x_0, y_0, z_0) represents the center position of the magnetic source, $\vec{B}$ is the regional value of the magnetic field, and η is the structural index. This structural index (η) is a measure of the rate of decay of the magnetic anomaly with the distance between the source and the measurement point (Ravat 1996), that is, an indicator of the geometric shape of the anomalous source. Each value of η is used for different geometric shapes of the structural of interest as shown in Table II.

Table II. Structural index (η) to each geometic form to Magnetic data by Thompson (1982).

η	Geometric form
0	Contact
1	Vertical Dike or Sill
2	Horizontal or Vertical cylinder
3	Sphere (dipolos)

Spectral Analysis of Crustal Magnetic Field

The determining of magnetic sources depths by spectral analysis of the anomalous magnetic datum (Spector & Grant 1970, Bhattacharyya & Leu 1977), is based on the assumption that the observed anomalous magnetic field is produced by a set of prismatic sources distributed in the crust. So that the logarithm of the average power spectrum generated by these anomalous magnetic sources in a given area is related to the depths of the top of the array, according to the equation below:

$$|F(k)|^2 = 4\pi^2 C_m^2 |\theta_m|^2 |\theta_f|^2 M_0^2 e^{-2kz_t} * \left(1 - e^{-k(z_b - z_t)}\right)^2 S^2(a, b) \tag{7}$$

where k is the wavenumber ($\frac{cycles}{km}$), C_m a constant, θ_m an angle related to the magnetization direction and θ_f an angle related to principal magnetic field direction in the final phase of acquisition data. M_0 is the magnitude of the magnetization vector, z_t and z_b are the top and bottom depths of magnetic sources. $S^2(a, b)$ is a factor related to horizontal dimensions of the anomalous magnetic source.

Therefore, the slope of the adjusted lines over power spectrum generated of anomalous magnetic sources is related to the depth of the top of this analyzed layer. These spectra can relate a peak frequency (or wavenumber) to the thickness of the original magnetic layer. In the Centroid method, the model is centred on collections of random samples of a uniformed distribution of prisms with constant magnetization. Thus, equation 7 is adjusted in terms that involve z_t and z_b in a hyperbolic sine function (Blakely 1996), plus a Centroid factor and for long wavelengths, the hyperbolic sine function tends to one, leaving only the Centroid term, thus:

$$|F(k)|^2 \sim Ce^{-kz_0}\Delta z.k \tag{8}$$

In the methods proposed by Bhattacharyya & Leu (1977) and Okubo et al. (1985), the estimates of the depth of the magnetized layer center (z_0) are obtained from the slopes of azimuthally averaged and the wavenumber scaled Fourier spectra in the low wavenumber region following the relation:

$$G(k) = \frac{1}{k}F(k) \tag{9}$$

Once the depth of the top of the deepest layer (z_t) is estimated from the amplitude spectrum, it is fairly simple to use the scaled amplitude spectrum to estimate the Centroid depth (z_0). The bottom depth (z_b) is then obtained using the equation 10:

$$z_b = 2z_0 - z_t \tag{10}$$

RESULTS AND DISCUSSION

Muriaé Watershed Geothermal Analysis

The geothermal database used in this research consisted of eight (8) direct measurements (thermal profiles) located near the basin and available in the LabGeot/ON collection (Geothermal Laboratory of the National Observatory) and twenty-two (22) well with groundwater information as part of the Groundwater Information System (SIAGAS by CPRM). The geographic distribution of these well is indicated in Figure 2. The geothermal gradient was calculated on both data using the CBT methodology described above.

With the geothermal gradient calculated a grid of the distribution was constructed to basin, using the *kriging* interpolation technique available in Oasis Montaj software. The map in Figure 3 shows the distribution of the geothermal gradient of the Muriaé watershed.

In this map, cool colors indicate more thermally stable regions with low heat flow in the surface and geothermal gradient below 20 $\frac{^0C}{km}$, as in the mid-western part of the basin, which is marked by the Pomba-Muriaé interplanaltic depression. The warm colors represent thermal anomaly areas with values for geothermal gradient above 40 $\frac{^0C}{km}$ specially in the southeastern part. It is possible to observer a geothermal gradient values greater than 25$\frac{^0C}{km}$ occur along the main drainage area of the river, with NW-SE direction.

For the surface temperature values (T_0), the average annual temperature measured at the surface in the last 30 years, provided by INMET, was taken into consideration. With the objective of analyzing the variations of thermophysical properties on a regional scale, was used the lithology profiles to calculate the mean thermal conductivity values. The profiles used has come of SIAGAS well (22) that had this information. The mean thermal conductivity, were estimated using the weighted average methodology. This procedure allowed the structuring of a database on thermal conductivity for the *Muriaé* basin.

It was possible to calculate the heat flow distribution from equation 2, mentioned above, multiplying the geothermal gradient values with the thermal conductivity. This set of values allowed the elaboration of a representative heat flow map in the basin, presented in the Figure 4. In this figure, it can be seen that the flow has a behavior similar to the geothermal gradient illustrated in Figure 3.

Knowing that the global mean heat flow values vary between 53-63 $\frac{mW}{m^2}$, according to Hamza & Vieira (2018), the heat flow values above this average ($>$80$\frac{mW}{m^2}$) can be considered positively anomalous
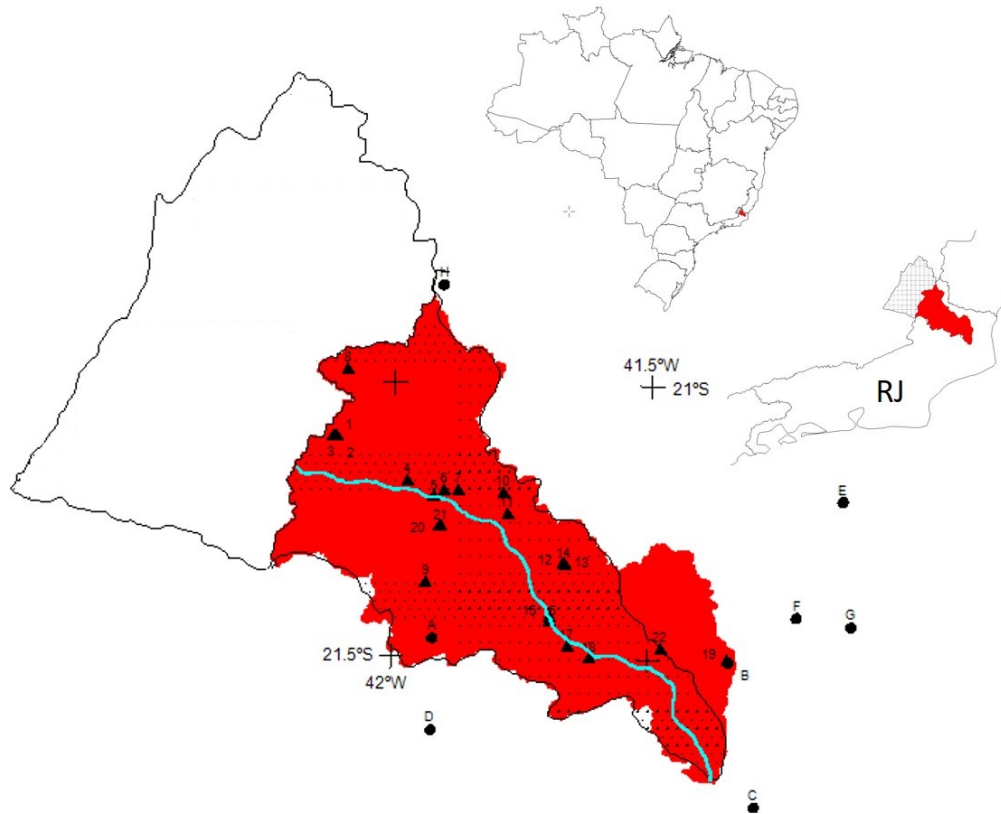
Figure 2. Geothermal database distribution using in this work. The red area indicate the Muriaé watershed in Rio de Janeiro state. The black triangles (A,B,C,D,E,F,G and H) indicate the SIAGAS well used in this word, the black circles (1-22) indicate the LabGeot/ON well.
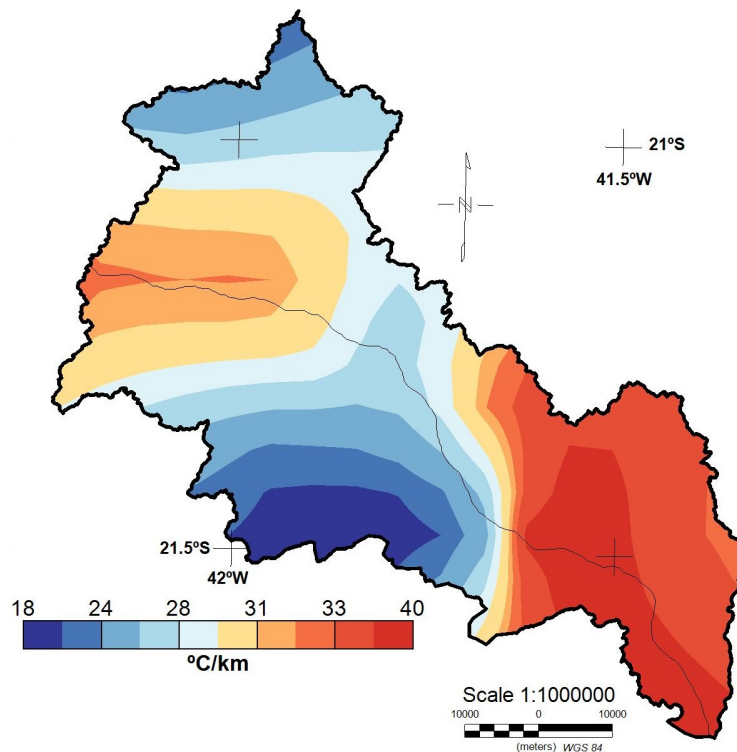
Figure 3. Geothermal gradient map of Muriaé watershed (Rio de Janeiro part).

values. These values are restricted to the SE portion of the basin, marked by lithology with low thermal conductivity values because it is the edge of the sedimentary basin of Campos. In the central-western part of the basin, marked by the Pomba-Muriaé interplanaltic depression, the heat flow values are similar to the global average, approximately 60 $\frac{mW}{m^2}$.

The Table III presents the summary of information on the geothermal parameters used and calculated in the thermal study of the basin.

Table III. Geothermal synthesis of *Muriaé* watershed. *ID* column indicates geothermal data information coming: direct measurements (A-H) and indirect estimates (1-22), the localization is illustrated in Figure 2; latitude (Lat) and Longitude (Long) were geographical coordinates in decimal degree; Γ is the geothermal gradient in $\frac{^0C}{km}$; λ is the thermal conductivity in $\frac{W}{mK}$ and *q* are the heat flow in $\frac{mW}{m^2}$.

ID	Lat	Long	Γ	λ	q	ID	Lat	Long	Γ	λ	q
A	-21.466	-41.920	25.7	2.8	72.0	8	-20.979	-42.093	25.0	2.9	72.5
B	-21.501	-41.342	21.3	2.7	57.5	9	-21.366	-41.936	23.7	3.3	78.2
C	-21.764	-41.286	27.1	2.7	73.1	10	-21.201	-41.787	26.0	2.5	66.3
D	-21.634	-41.920	25.5	2.6	66.4	11	-21.239	-41.778	28.0	2.7	75.6
E	-21.203	-42.125	18.4	3.0	55.1	12	-21.328	-41.668	26.7	3.0	79.2
F	-21.417	-42.211	20.1	3.0	60.4	13	-21.328	-41.665	34.0	2.7	90.8
G	-21.431	-42.104	15.5	3.0	46.6	14	-21.329	-41.665	35.5	2.5	92.5
H	-20.821	-41.909	14.6	2.9	42.2	15	-21.426	-41.693	26.9	2.8	75.2
1	-21.101	-42.119	29.2	3.1	89.4	16	-21.434	-41.692	21.5	2.8	60.3
2	-21.102	-42.115	30.8	2.5	78.5	17	-21.479	-41.657	25.8	2.8	72.3
3	-21.101	-42.113	33.3	2.5	85.0	18	-21.500	-41.614	37.8	2.8	105.0
4	-21.180	-41.974	32.0	2.7	86.4	19	-21.498	-41.345	32.5	2.7	87.8
5	-21.209	-41.922	33.3	2.7	90.0	20	-21.262	-41.910	25.9	2.8	72.6
6	-21.198	-41.902	30.0	2.7	80.1	21	-21.263	-41.908	33.3	3.1	103.3
7	-21.197	-41.875	28.0	2.5	71.4	22	-21.480	-41.475	34.0	2.5	86.7

From these calculated heat flow values described in Table III, the average value for the heat flow *Muriaé* watershed is the 74.4 $\frac{mW}{m^2}$.

Magnetic-Structural Framework of Muriaé Watershed

The Muriaé watershed, under study, is localized over the junction of two geographical sheets: UTM23S and UTM24S. Therefore, two aeromagnetic databases obtained between 2010 and 2012 were used: the Rio de Janeiro survey (code 1117) and the Espírito Santo survey (code 1093) (Brasil 2012, 2010). Both database were provided by CPRM to LabGeot/ON and are part of the airborne geophysical data collection of this laboratory. The main characteristics of these database are shown in Table IV.

According to the project report, in both airborne surveys, the aeromagnetometer was used for the magnetometric measurements assembled on the tail of the aircraft (stringer type). The readings from

Table IV. Characteristics of aeromagnetic database used in this research.

Project	Espirito Santo	Rio de Janeiro
Code	1093	1117
Geophysical Information	Magnetometry	Magnetometry
Flight height	100 m	100 m
Acquisition year	2010	2012
Lines spacing	500 m	500 m
Tie lines spacing	10 km	10 km
Lines direction	N-S	N-S
Tie lines direction	E-W	E-W
Sample	0.1 s	0.1 s

these magnetometers are taken every 0.1 second, which is equivalent, for an average acquisition speed of 270 $\frac{km}{h}$, to approximately 7.5 meters on the ground. These database have already been provided with preliminary field corrections, including the separation of their sources.

The anomalous magnetic field (AMF) values, which is of interest in this study, have also been delivered leveled (using the control lines) and micro-leveling. Thus, with the aeromagnetic data distributed throughout the study area, the process of generating regular grids for further interpretation was performed. The method of data interpolation used was that of least curvature (Smith & Wessel 1990).

A value of 200m was used for the interpolation spacing for all magnetometric maps. The AMF map represented in the Figure 5 allowed the identification of the regional magnetic characteristics of the Muriaé watershed. In the map, can observe considerable intensity variations. The $\pm$ 150nT value was obtained as the range of the AMF of the basin.

The south-central region of the basin is considered a magnetic low with NE-SW zones. The NW region, where there is a condensed fracturing zone according tectonic distribution and geological map, also has magnetic highs with NE-SW.

For detailing and highlighting of the structural magnetic sources of interest a high-pass filter was applied to the AMF grid. These sources are connected to linear structures which, in turn, are concomitant with geostructural lineaments.

The main tectonomorphic structures here and elsewhere at the surface are delimited and identified by yellow dotted lines in Figure 6, based on Silva (2002), which show these magnetic lineaments identified from the vertical derivative technique.

The magnetic lineaments mapped from the vertical derivative shading (30^0 illumination) show that predominant direction of these lineaments is NE-SW. The NW region of the basin is an area with high topographies related to the Atlantic plateau. Adjacent to the central area of the basin was found a condensed zone of the magnetic lineaments with small variations in their distances. This fact may suggest that this zone suffered an abrupt cooling during its formation.
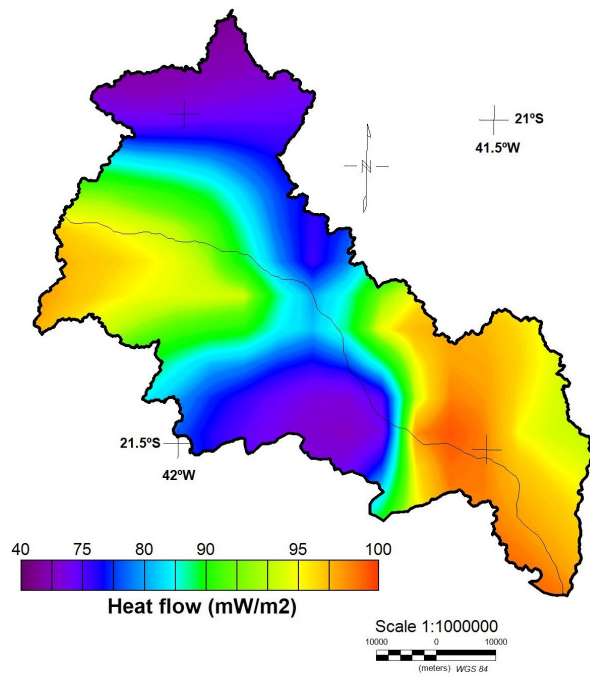
Figure 4. Heat flow distribution map of Muriaé watershed.
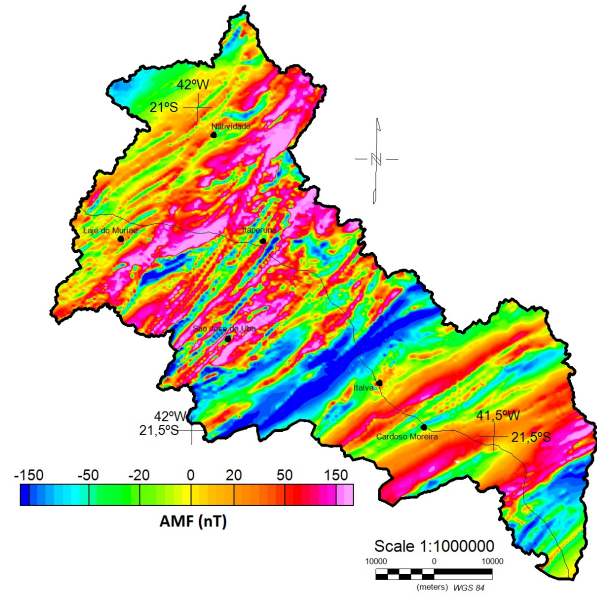
Figure 5. Anomalous Magnetic Field Map of Muriaé Watershed.
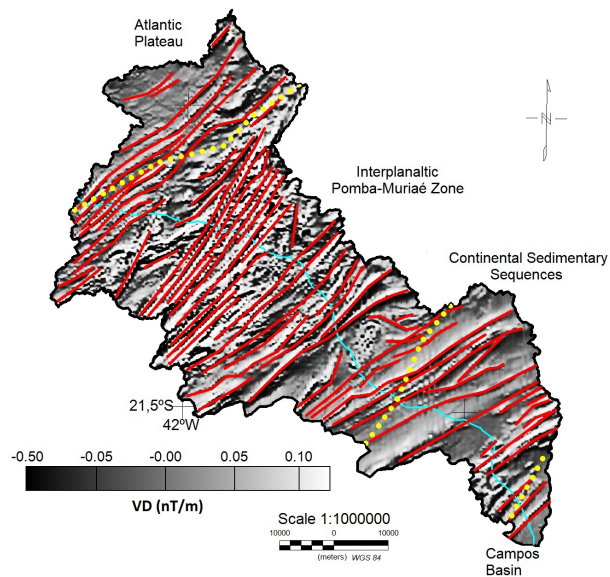
Figure 6. Vertical Derivative of AMF Map from Muriaé watershed. Yellow dotted lines represent the main morphostructural structures according to Silva (2002). Magnetic lineaments is in red.

In the SE region, it was possible to verify that the magnetic lineaments is more distant in comparison to central area and undergo a small movement to the east, coinciding with the tectono-structural context of the sedimentary sequences up to the edge of the Campos sedimentary basin, which the Muriaé river flows into the Paraíba do Sul river.

The Figure 7 provides a comparison between the results of different interpretive geophysical techniques (analytical signal amplitude, Euler deconvolution and spectral analysis) in the analysis of the spatial distribution and depths of magnetic sources related to the magnetic lineaments traced.

(a)   **(b)**   **(c)**
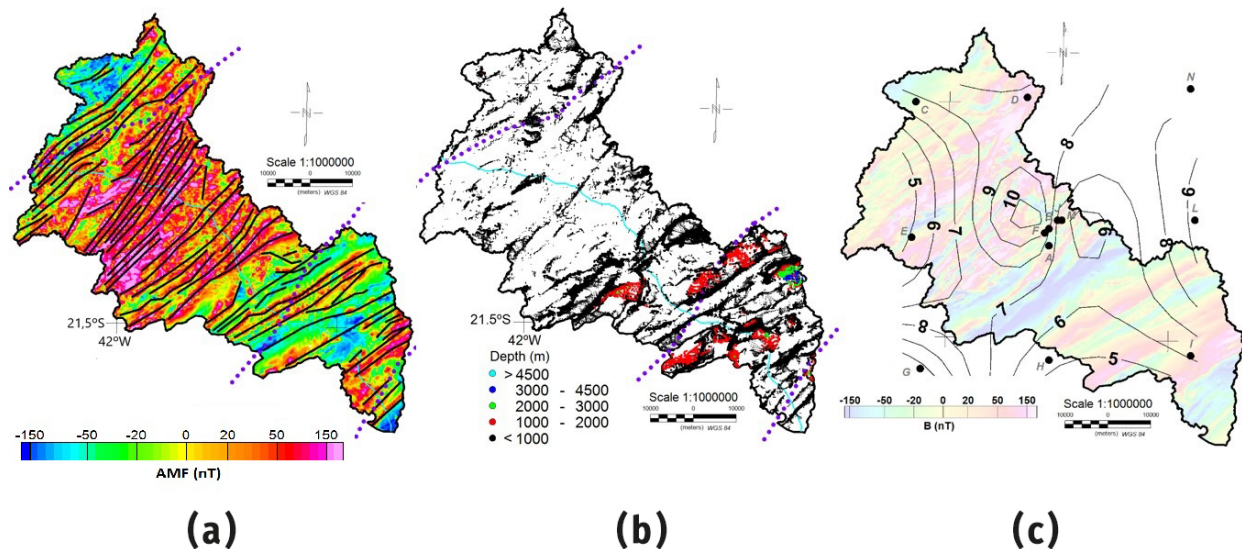
Figure 7. Maps of: (a) Analytical signal amplitude with the magnetic lineaments superimposed showing good spatial correlation; (b) Euler solutions applied to the AMF filtered grid revealing the depth of the shallow magnetic sources linked to structural index 1 (lineaments) and (c) Depth of magnetic sources obtained by spectral analysis of the AMF filtred (high-pass filter).

Interpretative techniques of vertical derivative and analytical signal amplitude were applied to the filtrated AMF, aiming to interpret anomalies associated with faults and dikes, enhanced through these techniques. The Euler deconvolution technique was used to verify the depths of these sources and, simultaneously, spectral analysis for the delimitation of the source depth. Such attributes were manipulated in the form of maps. The results of filtrated AMF and source depth are shown in part (c) of Figure 7.

In our study, to investigation about depth of magnetic sources, we used values of the anomalous magnetic field filtered to high frequency. This filtered field is correlated to the shallower sources in the crust corresponding to the magnetic lineaments previously traced using the vertical derivative technique. Therefore, these depths found are correlated with these shallower structures, in relation to sources that limit the magnetic crust.

The amplitude map of the analytical signal applied to the AMF filtered, illustrated in part (A) of Figure 7, also corroborates to the study of the magnetic-structural framework of the Muriaé basin. As it is possible to assess the region a degree of conformity with the linear structures identified in the vertical derivative map. The amplitude values of the analytical signal range from 0.01 to 0.30 $\frac{nT}{m}$.

To detail the depths of these structures, it structural index 1 was used (which is related to the dike models) in the Euler deconvolution technique and the maximum error of 10% for the position and depth of the sources (error factor inserted in the Oasis Montaj software), as shown in part (B) of Figure 7. The values found to the depth of these sources range from surface up to 4500m with a higher concentration of structures in the interval between 1000 and 1300m.

Unlike the Euler deconvolution technique, which selects only one source, different depth magnetized layers were identified using the spectral analysis methods. These methods select movable windows in the AMF filtered grid and calculate the depth of these magnetized layers from the selection a range of the wavelength (or frequency), centering the results on a point in the center of this window. In this way, the model generates a power spectrum based on the logarithm of this magnetic amplitude versus wavenumber for each selected window. The higher the wavenumber in the spectrum, the closer to the surface is the anomalous source. Thirteen regular windows with sizes ranging from 20 to 100m were used. The map represented in part (C) of Figure 7 illustrates this surface in the Muriaé basin through isolines, arranged in kilometers (km).

The deepest magnetic sources, according to this methodology, were found in the center region of the basin, where their depth varies from 3-8km approximately and are linked to the fracturing zone of the region. In the SE region of the study area, it was verified the existence of more punctual magnetic sources, with depth values approximately 4-5km. This characteristic comes from the sedimentary context of this area.

From the geothermal analysis performed at the thirty (30) geothermal points analyzed in conjunction with the geophysics techniques applied to the magnetic anomaly data, important results were achieved in the thermostructural characterization of the region. In this process, it was possible to separate the basin into two distinct thermomagnetic areas (Figure 8).

The Figure 8 shows two distinct thermostructural regions highlighted: Area 1 and Area 2. Area 2b related to the NW region of the study area has similar characteristics to Area 2, however, the data scarcity around the region makes it impossible to detailing its characterization.

Area 1, has a heat flow value within the global average, approximately 60 $\frac{mW}{m^2}$. Furthermore, this region is marked by lineaments with magnetic sources of depths between 3-8km, NNE-SSW direction and small separations between them. Aggregating these results to the local geology, marked mainly by the Pomba-Muriaé interplanaltic depression, an intense shear zone, tectonic framework marked by large lineaments (which coincide with the directions of the magnetic lineaments) and high degrees of fracturing. It was also evidenced that this area is geothermally stable zone. The cooling in its formation occurred abruptly and the high degree of fracturing does not characterize the current tectonic activities.

The Area 2, has anomalous heat flow values, around 80 $\frac{mW}{m^2}$, and a trend of more distant lineaments from each other, with ENE-WSW directions. In addition, its depths of the magnetic sources using spectral analysis in the AMF filtered is between 4-5 km. Geologically it is an area characterized by terracing and fluvial and/or fluvial-marine plains, where the marine transgression has raised the overall base level and there has been an intensive discharge of fluvial and marine sediments. The set of results, both geophysical and geological analyses, demonstrates that this region is a geothermal anomalous area. This is justified by the fact that the magnetic sources (lineaments, in this case) are at shallower depths.
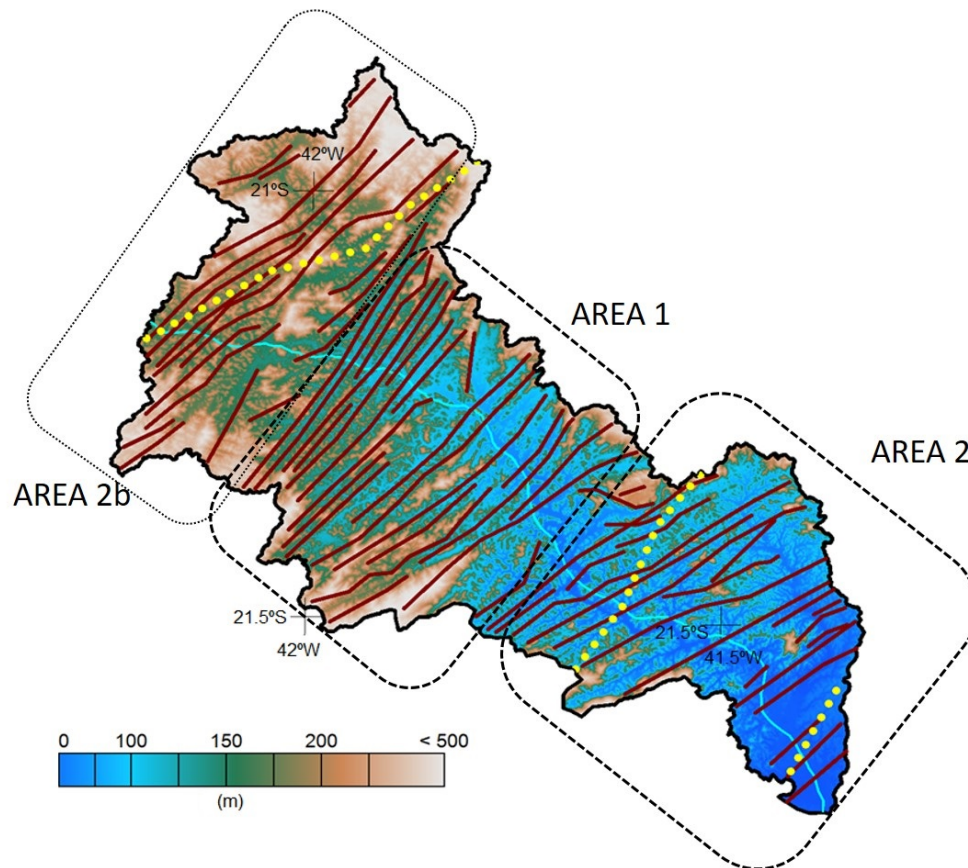
Figure 8. Topographic map of the Muriaé watershed with the discrimination of two distinct thermostructural areas found in this work.

CONCLUSIONS

The study area is marked by part of the Atlantic orogenic belt, a morphostructural unit that comprises a diverse set of metamorphic and igneous rocks of Precambrian and Paleozoic age. The tectonic of this region is mainly marked by a series of coastal massifs, faults and fractures (NE-SW in the central southern portion and NNE-SSW in the central northern portion) that contain some plateau zones and interplanaltic depression.

The geological units that mark the study region are predominantly the Araçuaí and Paraíba do Sul. Where there is the presence of Quaternary units formed by undifferentiated detrital coverings and the Barreiras unit. This group of rocks, with differential resistance to erosive process and denudation, gave origin to the mountain cliffs, the mounds and the hills present in the study area.

The structural lineaments evidenced on the surface were interpreted jointly with the identification of sixty-five (65) magnetic lineaments from airborne magnetic data interpretation. The depths of these structures were range from the surface up to 4.5 km.

The interpreted data allowed identification of regional tectonics features in the NE-SW direction, where the identified magnetic lineaments show a spatial correlation with accentuated topographic structures. The differences in the depths of the magnetic bodies found in conjunction with the

heat flow distribution, evidence two distinct thermostructural zones: A1 (east part) presenting heat flow values within the average (approximately $60\frac{mW}{m^2}$) and magnetic sources varying between 3-8 km in-depth. While the A2 (western), has anomalous heat flow ($80\frac{mW}{m^2}$ on average) and shallower magnetic sources, varying between 4-5 km.

Acknowledgments

REFERENCES

ALMEIDA FFM. 1976. The system of continental rifts bordering the Santos Basin, Brazil. An Acad Bras Cienc 48: 15-26.

AMORIM RR, REIS CH & FERREIRA C. 2017. Mapping of geosystems and anthropogenic systems as a subsidy for the study of areas at risk of flooding in the low course of the hydrographic basin of the Muriaé river (Rio of Janeiro - Brasil). Territorium 24: 89-114.

BENFENATTI MVC. 2017. Harnessing the geothermal potential in an underground mine: a literature review study. Monography - mining engineering graduation. Universidade Federal de Ouro Preto, MG, Brazil.

BHATTACHARYYA BK & LEU LK. 1977. Spectral analysis of gravity and magnetic anomalies due to rectangular prismatic bodies. Geophys 42(1): 41-50.

BIZZI LA, SCHOBBENHAUS C, VIDOTTI RM & GONÇALVES JH. 2003. Geology, Tectonics and Minerals Resources of Brazil: text, maps and GIS. CPRM, 692 p.

BLAKELY RJ. 1996. Potential theory in gravity and magnetic applications. Cambridge: Cambridge University Press, 461 p.

BOLDIZSAR T. 1958. New terrestrial heat flow values from Hungary. Geofis Pura Appl 39(1): 120-125.

BRASIL CSGD. 2010. Projeto Aerogeofísico Espírito Santo: relatório final do levantamento e processamento dos dados magnetométricos e gamaespectrométricos. Relatório Técnico - Prospectors Aerolevantamentos e Sistemas. Rio de Janeiro, Programa Geologia do Brasil (PGB).

BRASIL CSGD. 2012. Projeto Aerogeofísico Rio de Janeiro: relatório final do levantamento e processamento dos dados magnetométricos e gamaespectrométricos. Relatório Técnico - Prospectors Aerolevantamentos e Sistemas. Rio de Janeiro, Programa Geologia do Brasil (PGB).

BRENNER TL, FERRARI LA & PENHA HM. 1980. Northeastern structural lineaments of the Rio de Janeiro state. In: XXXI Congresso Brasileiro de Geologia, p. 2551-2564. SBG.

BULLARD EC. 1939. Heat flow in South Africa. Proceed Royal Soc London Math Phys Eng Sci 173(955): 474-502.

CERRONE BN & HAMZA VM. 2003. Paleoclimatic variations in the Rio de Janeiro state based on geothermal method. In: 8th International Congress of the Brazilian Geophysical Society. Rio de Janeiro, Brazil: European Association of Geoscientists & Engineers, p. cp-168.

CLARK D. 1997. Magnetic petrophysics and magnetic petrology: aids to geological interpretation of magnetic surveys. AGSO J Aust Geol Geophys 17: 83-104.

COELHO NETTO A. 1997. Geo-hydroecological mechanisms and conditions of silting in rural environment: implications for hillside stability. In: XXVI Congresso Brasileiro de Ciências do Solo. Rio de Janeiro, Brazil.

DANTAS ME. 2001. Geomorphology of Rio de Janeiro state, Brazil. Brasília: CPRM. Estudo Geoambiental do Estado do Rio de Janeiro, 75 p.

GOMES AJL & HAMZA VM. 2003. Evaluation of geothermal resources in the Rio de Janeiro state, Brazil. In: 8th International Congress of the Brazilian Geophysical Society. European Association of Geoscientists & Engineers, p. cp-168.

GUNN PJ. 1975. Linear transformations of gravity and magnetic fields. Geophys Prospect 23(2): 300-312.

HAENEL R, STEGENA L & RYBACH L. 1988. Handbook of Terrestrial Heat-Flow Density Determination. Springer, 485 p.

HAMZA VM & MUÑOZ M. 1996. Heat flow map of South America. Geothermics 25(6): 599-646.

HAMZA VM & VERMA RK. 1969. The relationship of heat flow with age of basement rocks. Bull Volcanol 33(1): 123-152.

HAMZA VM & VIEIRA F. 2018. Global heat flow: New estimates using digital maps and GIS techniques. Int J Terrest Heat Flow Appl Geotherm 1(1): 6-13.

HEILBRON M. 1995. The central segment of Ribeira Orogenic Belt: geological synthesis and geotectonic evolution test. Braz J Geol 25(4): 249-266.

KEAREY P, BROOKS M & HILL I. 2009. Exploration Geophysics. São Paulo: Oficina de Texto, 422 p.

KELLOGG OD. 1953. Foundations of Potential Theory. Vol. 31. Massachussetts: Courier Corporation, 384 p.

LI X. 2006. Understanding 3D analytic signal amplitude. Geophys 71(2): L13-L16.

NABIGHIAN MN. 1972. The analytic signal of two-dimensional magnetic bodies with polygonal cross-section: its properties and use for automated anomaly interpretation. Geophys 37(3): 507-517.

NABIGHIAN MN. 1984. Toward a three-dimensional automatic interpretation of potential field data via generalized Hilbert transforms: Fundamental relations. Geophys 49(6): 780-786.

OKUBO Y, GRAF RJ, HANSEN RO, OGAWA K & TSU H. 1985. Curie point depths of the island of Kyushu and surrounding areas, Japan. Geophys 50(3): 481-494.

PRADO RB, DANTAS ME, FIDALGO ECC, GONÇALVES AO, SILVEIRA MML, GUIMARÃES PV, FERRAZ RPD, MANSUR KL, VIEIRA H & DOURADO F. 2005. Diagnosis of the physical environment of the Muriaé watershed. Rio de Janeiro: Embrapa Solos-Documentos (INFOTECA-E), 76 p.

RAVAT D. 1996. Analysis of the Euler method and its applicability in environmental magnetic investigations. J Environ Eng Geophys 1(3): 229-238.

REID AB, ALLSOP JM, GRANSER H, MILLETT AJT & SOMERTON IW. 1990. Magnetic interpretation in three dimensions using Euler deconvolution. Geophys 55(1): 80-91.

RICCOMINI C. 1989. The continental rift of southeastern Brazil. Ph.D. thesis. Universidade de São Paulo.

ROEST WR, VERHOEF J & PILKINGTON M. 1992. Magnetic interpretation using the 3-D analytic signal. Geophys 57(1): 116-125.

SADOWSKI GR & CAMPANHA GADC. 2004. Major faults in continental Brazil. Geologia do Continente Sul-Americano: Evolução da Obra de Fernando Flavio Marques de Almeida, p. 373-407.

SALVIANO MF. 2019. Hydrological modeling of the Muriaé watershed with TOPMODEL: telemetry and remote sensing. Ph.D. thesis. Universidade de São Paulo, 163 p.

SILVA T. 2002. The geomorphological structuring of the Atlantic plateau in the Rio de Janeiro state. Ph.D. thesis. Universidade Federal do Rio de Janeiro, 265 p.

SMITH WHF & WESSEL P. 1990. Gridding with continuous curvature splines in tension. Geophys 55(3): 293-305.

SPECTOR A & GRANT FS. 1970. Statistical models for interpreting aeromagnetic data. Geophys 35(2): 293-302.

SWANBERG CA & MORGAN P. 1980. The silica heat flow interpretation technique: assumptions and applications. J Geophys Res: Solid Earth 85(B12): 7206-7214.

THOMPSON DT. 1982. EULDPH: A new technique for making computer-assisted depth estimates from magnetic data. Geophys 47(1): 31-37.

ÖZISIK MN. 1993. Heat Conduction. 2nd ed. New York, US: Wiley & Sons Inc, 712 p.

SUZE N.P. GUIMARÃES[1]
https://orcid.org/0000-0002-0867-1058

FÁBIO P. VIEIRA[1]
https://orcid.org/0000-0002-8004-9298

HELLEN R. BARBOZA[2]
https://orcid.org/0000-0003-0478-6648

[1]Observatório Nacional (ON/MCTI), Departamento de Geofísica, Laboratório Geotérmico (LabGeot/ON), Rua General José Cristino, 77, São Cristóvão, 20921-400 Rio de Janeiro, RJ, Brazil
[2]Universidade Federal Fluminense (UFF), Institute de Geociência, Departamento de Geologia e Geofísica (GGO), Av. Gal. Milton Tavares de Soua, s/n, Campus da Praia Vermelha, Boa Viagem, 20210-346 Niterói, RJ, Brazil

Correspondence to: **Suze Nei Pereira Guimarães**

E-mail: suze@on.br

Author contributions

Suze Nei Pereira Guimarães: Main author, conception and design of study, acquisition of data, discussion of results (analysis and interpretation of data), drafting the manuscript, revising the manuscript critically for important intellectual content, Approval of the version of the manuscript to be published and the reviews. Fábio Pinto Vieira: conception and design of study, acquisition of data, discussion of results (analysis and interpretation of data), approval of the version of the manuscript to be published and the reviews. Hellen Rosa Barboza: Conception and design of study, discussion of results (analysis and interpretation of data), interpretation of reviews, data processing and use results in undergraduate work.